Journal of Materials Chemistry

Cite this: J. Mater. Chem., 2012, 22, 6117

www.rsc.org/materials

PAPER

Sol–gel emulsion synthesis of biphotonic core–shell nanoparticles based on lanthanide doped organic–inorganic hybrid materials†

Xianmin Guo,[bc] Jean-Louis Canet,[ac] Damien Boyer,*[ac] Arnaud Gautier*[bc] and Rachid Mahiou[bc]

Received 26th October 2011, Accepted 9th January 2012
DOI: 10.1039/c2jm15470f

Eu^{3+} and Tb^{3+} complexes based on an organo-alkoxysilane derived from 4-azido dipicolinic acid by "click chemistry" were coated onto silica nanoparticles previously prepared by the water in oil emulsion method. Structural and optical properties of the resulting luminescent core–shell monodisperse (30 nm) nanohybrids were fully characterized by infrared and Raman spectroscopies as well as by electron microscopy. Fluorescence spectroscopy evidenced that an efficient ligand-to-Ln^{3+} energy transfer—both in the mono- and biphotonic modes—occurs. Furthermore, surface modification by amino groups was realized, paving the way for nanotags of biological interest.

Introduction

Within the past ten years, the development of fluorescent silica-based nanoparticles has aroused great scientific and technological interest for bioanalysis and biotechnological applications since they exhibit many more advantages in comparison with free fluorophores, quantum dots or fluorescent polymer-based nanoparticles (NPs).[1] Indeed, the use of a silica matrix to encapsulate a luminescent dye prevents any problems of bleaching, blinking, leaching, hydrophobicity or biocompatibility.[2] Regarding surface functionalization of such luminescent NPs, specific functional groups (*e.g.* amine, thiol, carboxylic acid) can be easily grafted using various organoalkoxysilanes allowing us to link a broad range of biorecognition agents (such as nucleic acids, antibodies or proteins).[3]

Among the various types of fluorescent sources available today, lanthanide (Ln^{3+}) complexes appear as the most attractive since they exhibit outstanding optical properties:[4] long luminescence lifetime (hundreds of microseconds), large Stokes shift (>150 nm) and narrow emission bands (<10 nm).[4] However, as Laporte selection rules forbid f–f transitions of Ln^{3+} ions, organic ligands are required to attain high luminescence quantum efficiencies. This latter characteristic results from the intense absorption band of organic chromophores and an efficient organic ligand-to-Ln^{3+} energy transfer by the so-called antenna effect.[5] Consequently, the key factor to obtain strong luminescence is to design and prepare conjugated organic ligands (*e.g.* β-diketonates, aromatic carboxylates or heterocyclic systems) that possess an excited triplet state T_1 well matching the high excited states of the central Ln^{3+} ion.[6] Among them, dipicolinate (DPA) derivatives constitute a class of popular ligands presenting strong absorption coefficients and efficient transfer of absorbed energy to the central Ln^{3+} ions.[7] Their maximum absorption wavelengths may be tuned by changing the attached group in position C-4 (Fig. 1) as we and others have recently demonstrated through a simple "click chemistry" process.[8] Click chemistry, particularly thanks to the copper-catalyzed azide–alkyne cycloaddition (CuAAC), brought new vitality to various fields of research since its concept was introduced in 2001 by Meldal and Sharpless.[9] Its prominent and popular features include simple and mild reaction conditions, high yield, easy isolation and few byproducts thus opening a wide range of novel and exciting opportunities for new materials design. To date, this "click" reaction has been used for the preparation of functional

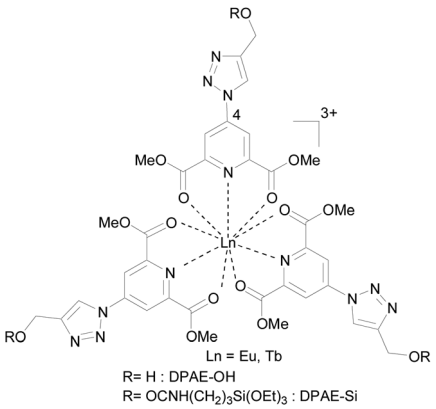

Fig. 1 Europium and terbium complexes of DPA derivatives.

[a]*Clermont Université, ENSCCF, Institut de Chimie de Clermont-Ferrand, BP 10448, F-63000 Clermont-Ferrand, France. E-mail: damien.boyer@ensccf.fr; Fax: +33 (0)4-73-40-71-08; Tel: +33 (0)4-73-40-76-47*
[b]*Clermont Université, UBP, Institut de Chimie de Clermont-Ferrand, BP 10448, F-63000 Clermont-Ferrand, France. E-mail: Arnaud.Gautier@univ-bpclermont.fr; Fax: +33 473-40-77-17; Tel: +33 473-40-76-46*
[c]*CNRS, UMR 6296, ICCF, F-63177 Aubière, France*
† Electronic supplementary information (ESI) available. See DOI: 10.1039/c2jm15470f

polymers, modification of surfaces, diversity of drugs, and so on.[10] However, to the best of our knowledge, the fabrication of DPA derivatives based on the CuAAC reaction and their applications in the field of lanthanide luminescence have been rarely reported.[8]

In this manuscript we propose luminescent hybrid materials prepared by covalently grafting the lanthanide complexes $Ln(DPAE–Si)_3$ ({1-[2,6-di(methoxycarbonyl)pyridin-4-yl]-1*H*-1,2,3-triazol-4-yl}methyl 3-(triethoxysilyl) propyl carbamate; Ln = Eu and Tb; Fig. 1) onto the surface of pure silica NPs previously synthesized by reverse sol–gel emulsion. Further surface functionalization with amino groups ($–NH_2$) was carried out. The structural, morphological and optical properties of different materials were discussed in detail. Fluorescence microscopy upon ultraviolet (UV) and infrared (IR) excitation was achieved to assess the potentialities of these luminescent hybrid materials for biolabelling applications.

Results and discussion

Structural characterizations

Fig. 2 presents the FTIR spectra of DPAE–OH (a), DPAE–Si (b), SiO_2@Eu(DPAE–Si)$_3$ (c) and SiO_2@Tb(DPAE–Si)$_3$ (d).

Compared to Fig. 2a, new characteristic vibration bands are observed in Fig. 2b which are assigned to –OCONH– groups (C–N stretching and N–H bending at 1540 cm^{-1}) and C–Si–OEt (1391, 1104, 1078 and 795 cm^{-1}) groups, proving that the organic ligand DPAE–OH was successfully functionalized by 3-isocyanatopropyltrimethoxysilane (ICPTES), in good agreement with ^1H NMR results. In Fig. 2c and d, the formation of the Si–O–Si framework is confirmed by the broad absorption band centered at 1100 cm^{-1} (ν_{as}, Si–O) and the narrower one located at 795 cm^{-1} (ν_s, Si–O). Moreover, the characteristic band at 1540 cm^{-1} attributed to the –OCONH– groups can also be seen in both hybrid materials, suggesting that DPAE–Si remains intact in the whole procedure. SEM images of SiO_2@Ln(DPAE–Si)$_3$ (Ln = Eu^{3+} and Tb^{3+}) are displayed in Fig. 3.

It can be easily observed that both samples exhibit uniform spherical morphologies with an average diameter of about 30 nm. The corresponding TEM images further support the above statement, as shown in Fig. 4.

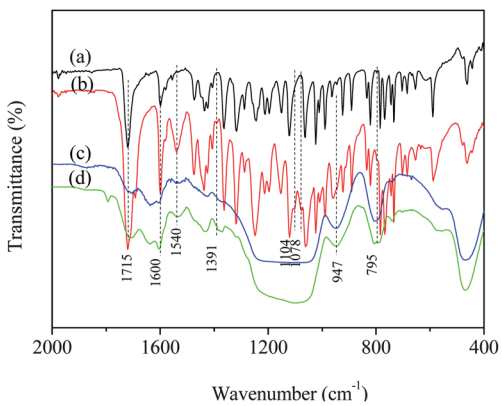

Fig. 2 FTIR spectra of (a) DPAE–OH, (b) DPAE–Si, (c) SiO_2@Eu(DPAE–Si)$_3$ and (d) SiO_2@Tb(DPAE–Si)$_3$.

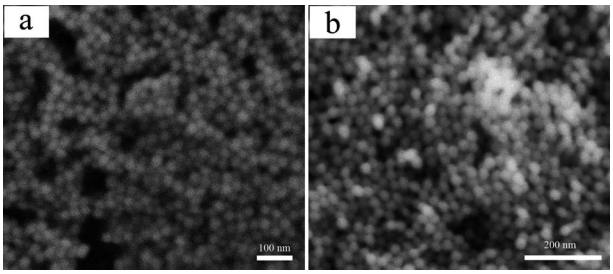

Fig. 3 SEM images of (a) SiO_2@Eu(DPAE–Si)$_3$ and (b) SiO_2@Tb(DPAE–Si)$_3$.

The TEM images of SiO_2@Ln(DPAE–Si)$_3$ (Ln = Eu^{3+} and Tb^{3+}) show spherical particles with uniform size distributions around 30 nm, in accordance with SEM investigation results. Although the core–shell structures for both materials could not be confirmed by the above-mentioned characterization methods owing to the limits of equipment, the luminescent properties coming from the characteristic Ln^{3+} ions evidence that Ln(DPAE–Si)$_3$ (Ln = Eu^{3+} and Tb^{3+}) complexes have been successfully grafted onto the surface of silica nanospheres. Furthermore, surface functionalization with amino groups could be realized using aminopropyl triethoxysilane (APTES). The Raman spectrum of APTES modified SiO_2@Eu(DPAE–Si)$_3$ nanoparticles (Fig. 5a) exhibits typical stretching vibrations of primary amines' N–H bonds located between 3250 and 3400 cm^{-1}. Furthermore, vibration bands ascribed to aliphatic ($–CH_3$) and acyclic ($–CH_2–$) groups are much stronger in Fig. 5b.

Photoluminescence studies

As discussed in the Introduction, the effective ligand-to-Ln^{3+} intramolecular energy transfer is one of the key factors for design of Ln-based luminescent hybrid materials. Fig. 6 exhibits the UV absorption spectra of the parent ligand DPAE–OH, functionalized ligand DPAE–Si, the resultant core–shell hybrid materials SiO_2@Ln(DPAE–Si)$_3$ (Ln = Eu^{3+} and Tb^{3+}) in ethanol, and the excitation spectra of SiO_2@Ln(DPAE–Si)$_3$ (Ln = Eu^{3+} and Tb^{3+}) as solid samples obtained by monitoring the emission wavelengths of Eu^{3+} and Tb^{3+} ions at 616 nm and 546 nm respectively.

Two absorption bands from 190 to 300 nm are easily observed in the UV absorption spectra of all samples (Fig. 6a–d), which can be attributed to transitions from the ground state (π) S_0 to the excited level (π^*) S_1 of organic ligands. Compared to the ligand DPAE–OH, the two absorption peaks for DPAE–Si separately shift from 216 and 265 nm to 213 and 260 nm. This

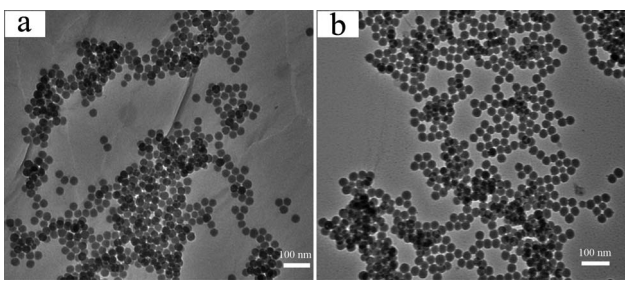

Fig. 4 TEM images of (a) SiO_2@Eu(DPAE–Si)$_3$ and (b) SiO_2@Tb(DPAE–Si)$_3$.

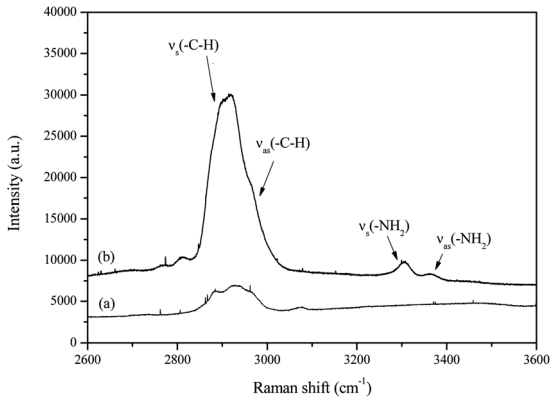

Fig. 5 Raman spectra of (a) SiO_2@Eu(DPAE–Si)$_3$ and (b) SiO_2@Eu(DPAE–Si)$_3$@NH_2.

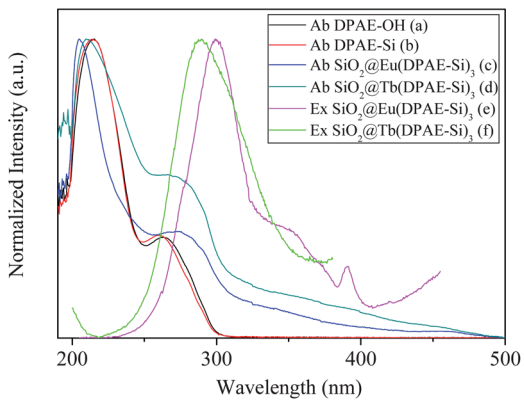

Fig. 6 UV-Vis absorption spectra of (a) DPAE–OH, (b) DPAE–Si, (c) SiO_2@Eu(DPAE–Si)$_3$ and (d) SiO_2@Tb(DPAE–Si)$_3$ at 1×10^{-4} mM in ethanol, respectively; excitation spectra of (e) SiO_2@Eu(DPAE–Si)$_3$ and (f) SiO_2@Tb(DPAE–Si)$_3$ were recorded at room temperature from solid samples by monitoring the red and the green fluorescence at 616 and 544 nm respectively.

weak blue-shift is probably due to a change in electron distribution in π and/or π* states of the functionalized ligand of DPAE–Si. Furthermore, the spectral shapes of SiO_2@Eu(DPAE–Si)$_3$ and SiO_2@Tb(DPAE–Si)$_3$ (Fig. 6c and d) are quite similar to those of free ligands (Fig. 6a and b), indicating that coordination of the Ln^{3+} ion to organic ligands does not have a remarkable influence on the π–π* energies. However, introduction of Ln^{3+} ions produces an increase of the crystal field manifested by a more pronounced splitting between the two bands. It should be noticed that an overlap clearly exists between the absorption band of DPAE–Si and the excitation bands of SiO_2@Ln(DPAE–Si)$_3$ (Ln = Eu^{3+} and Tb^{3+}) (Fig. 6e and f), suggesting that Ln^{3+} ions can be efficiently sensitized by the surrounding ligands through an "antenna effect".

For the excitation spectrum of SiO_2@Eu(DPAE–Si)$_3$, in addition to a broad excitation band of organic ligands between 250 and 400 nm, a sharp peak at 391 nm is also observed and assigned to intra-shell $^7F_0 \rightarrow {}^5L_6$ absorption transition of Eu^{3+} ions. Compared to the absorption intensity of organic ligands, this transition is much weaker, demonstrating that luminescence sensitization through excitation of the ligands is much more efficient than through direct excitation in highly excited energy levels of Eu^{3+} ions.

Fig. 7 exhibits the normalized emission spectra of SiO_2@Eu(DPAE–Si)$_3$ and SiO_2@Tb(DPAE–Si)$_3$ as solid samples recorded at room temperature upon excitation at the maximum excitation wavelengths namely 300 nm and 289 nm respectively. As shown in Fig. 7a, the emission spectrum of SiO_2@Eu(DPAE–Si)$_3$ is composed of the typical fluorescent lines of the Eu^{3+} ion at *ca.* 579, 591, 615, 651, and 695 nm, corresponding to the intra shell-4f^6 $^5D_0 \rightarrow {}^7F_J$ (J = 0, 1, 2, 3, and 4) transitions respectively, with the red $^5D_0 \rightarrow {}^7F_2$ emission as the dominant band. Moreover, a broad band with two peaks is also detected in the range of 410–570 nm (magnified in Fig. 7), which are attributed to the emissions arising from the triplet states of the organic ligands and the Eu^{3+} $^5D_1 \rightarrow {}^7F_{1-2}$ transitions, respectively. However, the emission intensity in the blue-green spectral region is much weaker in comparison with those of the $^5D_0 \rightarrow {}^7F_{0-4}$ transitions. As a consequence, the negligible intensity of this band clearly reveals that an efficient energy transfer occurs from the organic ligands to $^5D_0$-Eu^{3+} ions in the resultant core–shell hybrid materials.

In the case of SiO_2@Tb(DPAE–Si)$_3$, upon excitation in the absorption band of organic ligands, four characteristic emission bands of Tb^{3+} ions assigned to the $^5D_4 \rightarrow {}^7F_{3-6}$ transitions are observed, which locate respectively at 488, 543, 583, and 620 nm. At the same time, the $^5D_4 \rightarrow {}^7F_J$ (J = 2, 1, and 0) transitions at

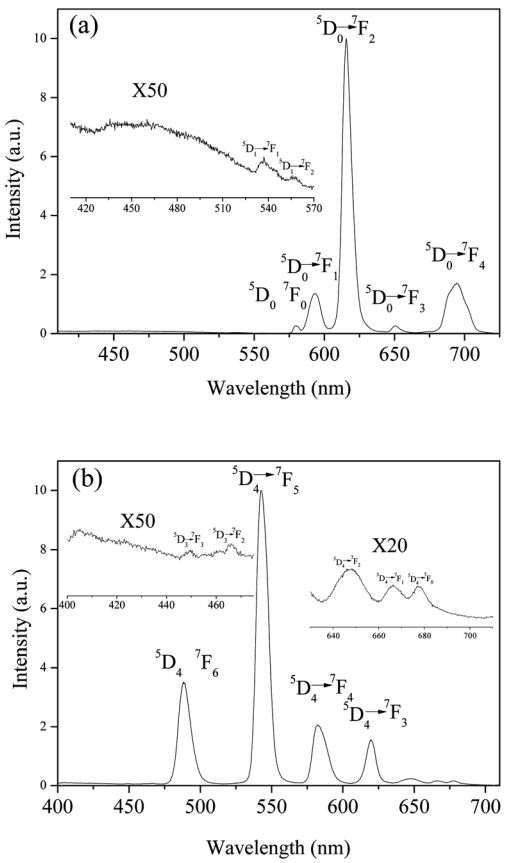

Fig. 7 Emission spectra of (a) SiO_2@Eu(DPAE–Si)$_3$ (λ_{ex} = 300 nm) and (b) SiO_2@Tb(DPAE–Si)$_3$ (λ_{ex} = 289 nm) recorded at room temperature.

648, 666 and 678 nm can also be detected in the amplificatory spectral range from 630 to 710 nm. Similarly to Eu^{3+}, the emission spectrum in the blue region of 410–475 nm was magnified and exhibits very weak Tb^{3+} $^5D_3 \rightarrow {}^7F_{2,3}$ transitions and a weak contribution of the organic ligand indicating that an efficient energy transfer occurs from this latter to $^5D_4$-Tb^{3+} ions in SiO_2@Tb(DPAE–Si)$_3$.

The luminescence decay times (τ_{exp}) of the $^5D_0$-Eu^{3+} excited level for SiO_2@Eu(DPAE–Si)$_3$ and of the $^5D_4$-Tb^{3+} excited level for SiO_2@Tb(DPAE–Si)$_3$ were recorded at room temperature using an excitation wavelength of 346.5 nm and by monitoring the most intense emission lines at 616 and 543.5 nm, respectively (Fig. 8).

Both decay curves are well fitted by a bi-exponential function with a long and a short time contribution like in DPAE:Eu^{3+} and DPAE:Tb^{3+} complexes. Such a behaviour indicates that Ln^{3+} ions (Ln^{3+} = Eu^{3+} or Tb^{3+}) exhibit two different local environments in each sample. The corresponding luminescence lifetimes were independently determined to be 0.60 ms and 0.27 ms for SiO_2@Eu(DPAE–Si)$_3$ and, 0.92 ms and 0.19 ms for SiO_2@Tb(DPAE–Si)$_3$. The long components for both samples fit well with those derived from the complexes while the short components are twice higher. Time resolved fluorescence line narrowing spectroscopy coupled to structure description is planned to explain these features and will be the subject of further experiments.

In order to assess the capabilities as a fluorescent probe for multiphoton microscopy, the near infrared (NIR) excitation spectrum of SiO_2@Eu(DPAE–Si)$_3$ was recorded at room temperature by monitoring the Eu^{3+} $^5D_0 \rightarrow {}^7F_2$ transition at 616 nm (Fig. 9).

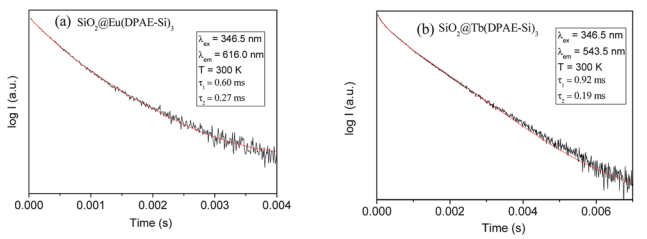

Fig. 8 Luminescence decay curves of (a) SiO_2@Eu(DPAE–Si)$_3$ and (b) SiO_2@Tb(DPAE–Si)$_3$ recorded at room temperature.

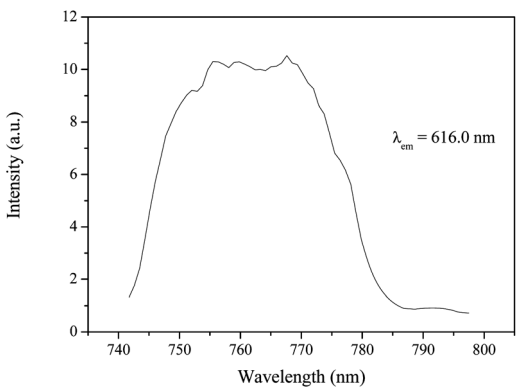

Fig. 9 NIR excitation spectrum of SiO_2@Eu(DPAE–Si)$_3$ recorded at room temperature by monitoring the Eu^{3+} $^5D_0 \rightarrow {}^7F_2$ transition at 616 nm.

The spectral repartition of this uncorrected spectrum from the response of the dye laser solution used fits quite well with the one photon excitation spectrum (OPE) recorded upon UV excitation monitoring the same fluorescence. Since the excitation values are twice the ones of the OPE spectrum, we assume that a two photon excitation (TPE) mechanism *via* the ligands takes place leading to the observation of the red fluorescence of the NPs. This observation indicates clearly the capability of such NPs to be utilized as TPE fluorescent probes.

Fluorescence microscopy analyses

In order to explore the potential applications of SiO_2@Eu(DPAE–Si)$_3$ and SiO_2@Tb(DPAE–Si)$_3$ in biological fields as nanotags, the resultant core–shell nanoparticles were imaged by fluorescence confocal microscopy with the available CW excitation at 405 nm (Fig. 10).

As expected, the images given in Fig. 10 exhibit strong red and green fluorescence with high signal-to-noise ratio, demonstrating that they fulfil the requirements for bio-labeling applications.

Conventional fluorescent labels, including semiconductor quantum dots and organic fluorophores, are mostly based on down-conversion, *i.e.* they are excited by ultraviolet (UV) or short wavelength visible (VIS) radiations. Hence, they have a very limited penetration in tissues because of scattering and absorption of optical photons. Furthermore, under UV or VIS excitation, a biological medium may produce strong autofluorescence from chromophores (*e.g.*, collagens, porphyrins, *etc.*), which decreases the sensitivity of detection. Finally, UV radiations have potential cytotoxic and carcinogenic effects, and are therefore not an attractive option for live cell/tissue imaging.

In contrast, fluorescent labels that are excited by NIR radiations give rise to minimal autofluorescence because of the lack of efficient endogenous absorbers in the NIR spectral range. Photodamage to cells and tissues is thus strongly reduced, and penetration depths are increased (notably in the windows 0.7–1.1 μm) by several orders of magnitude. As a result confocal and biphotonic microscopy is of great interest for medical applications. By using this technique, the image in Fig. 11 was recorded from SiO_2@Eu(DPAE–Si)$_3$ nanoparticles upon excitation at

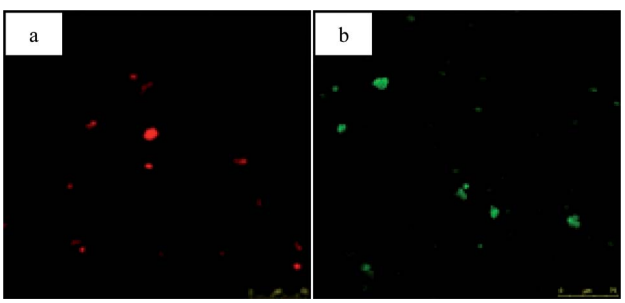

Fig. 10 Fluorescence microscopy images of (a) SiO_2@Eu–DPAE and (b) SiO_2@Tb–DPAE recorded upon laser excitation at 405 nm.

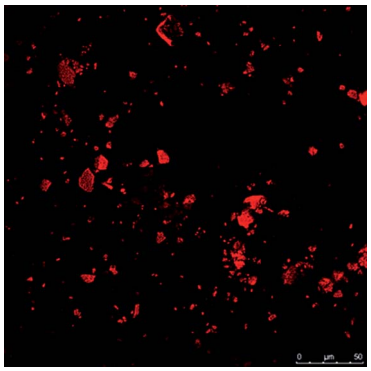

Fig. 11 Fluorescence microscopy image of SiO_2@Eu–DPAE recorded upon laser excitation at 750 nm in the NIR range.

750 nm demonstrating a contrast high enough for bio-labeling purposes.

Conclusions

A novel DPA derivative, DPAE, was synthesized *via* the "click chemistry" route and further silylated with ICPTES with high yield and simple reaction conditions. Based on DPAE–Si as a linker, luminescent core–shell nanoparticles SiO_2@Ln(DPAE–Si)$_3$ (Ln = Eu^{3+} and Tb^{3+}) were prepared by covalently grafting lanthanide complexes Ln(DPAE–Si)$_3$ onto the surface of pure silica nanoparticles. Surface functionalization with amino groups was achieved by the sol–gel process leading to SiO_2@Ln(DPAE–Si)$_3$@NH_2 (Ln = Eu^{3+} and Tb^{3+}) nanoparticles. The resultant materials present excellent luminescence and efficient energy transfer from the organic ligands to Ln^{3+} ions. At the same time, fluorescence of SiO_2@Eu(DPAE–Si)$_3$ was evidenced by confocal microscopy upon NIR excitation, demonstrating a great potentiality as biphotonic probes for biomedical imaging.

Further linkages to biocompatible and biorecognition agents are underway prior to performing biological tests.

Methods

Dimethyl 4-azidopyridine-2,6-dicarboxylate and DPAE–Si were synthesized according to the literature.[8a] All other chemicals and solvents were of analytic grade and used as received from Aldrich or Fluka.

Fourier transform infrared (FTIR) spectra were measured on a Perkin-Elmer 16PC spectrometer within the wavenumber range 4000–400 cm^{-1} at a resolution of 4 cm^{-1} with the KBr pellet technique. Raman spectra within the wavenumber range 3000–400 cm^{-1} were measured on a T64000 Jobin Yvon confocal microRaman spectrometer equipped with an Olympus microscope and a CCD detector cooled with liquid nitrogen. The 514.532 nm line of a Spectra Physics Stabilite 2017 Ar Laser operating at 100 mW was used as an excitation source.

Observations by transmission electron microscopy were performed on a Hitachi H-7650 at an acceleration voltage of 120 kV while SEM micrographs were recorded by means of a ZEISS Supra 55VP scanning electron microscope operating in high vacuum between 4 and 15 kV, using a secondary electron detector (Everhart–Thornley detector).

UV-Vis absorption measurements were carried out on a Nicolet Evolution 500 spectrophotometer with ethanol as the solvent.

The continuous wave (CW) photoluminescence spectra were collected using as excitation source a 450 W xenon lamp CW monochromatized through TRIAX 180 from Jobin-Yvon/Horiba and analyzed by a TRIAX 550 Jobin-Yvon/Horiba monochromator equipped with either a R928 Hamamatsu photomultiplier or a nitrogen-cooled CCD camera (Jobin-Yvon Symphony LN_2 series) as a detector. CW-excitation and emission spectra were obtained by monitoring the detector response while scanning the appropriate monochromator. The luminescence decays were obtained by pulsed excitation using a pulsed dye laser (Continuum ND60) pumped by a Continuum Surelite I-SL10 doubled Nd:YAG laser (10 ns pulse, 0.1 cm^{-1} band width, and 10 Hz repetition rate). The dye laser was followed by a H_2-Raman cell (for IR excitation) or a KDP frequency doubler (for UV excitation). LDS 698 used as dye solution provides energy up to 400 μJ in the doubled selected UV region or 4 mJ in the H_2-Raman Stokes shifted IR region. The frequency doubled or Raman shifted dye laser beam is spatially isolated from the fundamental dye laser beam by two Pellin–Brocca prisms associated with an iris diaphragm. In addition adequate sets of low or long pass-band filters are used to block any parasitic laser radiation. The red or green fluorescence of respectively Eu^{3+} and Tb^{3+} is analyzed through a Jobin-Yvon HR 1000 monochromator (focal length: 1 m, 1200 groove mm^{-1} grating and a band-pass of 8 Å mm^{-1} slits). The detector was a Hamamatsu R1104 photomultiplier tube. Fluorescence decays were measured with a Lecroy 9310A-400 MHz digital oscilloscope.

Regarding fluorescence microscopy, a Zeiss LSM 510 confocal scanning microscope was used to collect the images upon excitation at 405 nm while for the biphotonic study, a Leica SP5 confocal laser scanning microscope was utilized.

Synthesis of core–shell luminescent nanoparticles SiO_2@Ln(DPAE–Si)$_3$ (Ln = Eu^{3+} and Tb^{3+})

Silica nanoparticles were prepared according to a ternary reverse emulsion method based on the sol–gel process.[11] Firstly, 4.05 g (9.2 mmol) of polyoxyethylene(5) nonylphenyl ether (NP-5) were mixed in 93 mL (0.863 mol) of cyclohexane under magnetic stirring at room temperature. After the dissolution of the non-ionic surfactant for nearly 15 minutes, 420 μL (6.2 mmol) of concentrated ammonia were added to achieve the water-in-oil nanoemulsion. After further 15 minutes stirring, 2.3 mL (10.4 mmol) of tetraethylorthosilicate (TEOS) were added to initiate the reaction. The reaction was allowed to continue for 24 hours under stirring. To stop the reaction and isolate the particles, approximately 50 mL of acetone were slowly introduced into the emulsion: a white precipitate formed within the solution. Then the nanoparticles were collected by centrifugation at a speed of 3500 rpm for 20 minutes. Thereafter, the nanoparticles were washed twice with absolute ethanol in order to remove all the remaining surfactant. The silica particles were then dried in an oven at 80 °C for 24 hours. The mass yield of nanoparticles was found to be around 50% with regard to the initial TEOS quantity. Nanoparticles with an average diameter of 30 nm and

of monodisperse size have been evidenced by transmission electron microscopy.

Subsequently, Ln(DPAE–Si)$_3$ solution (0.01 M) was synthesized by dissolution of DPAE–Si and $Ln(NO_3)_3 \cdot 6H_2O$ in anhydrous ethanol (5 mL) with a molar ratio of Ln^{3+} : DPAE–Si = 1 : 3 under argon at room temperature and further stirring for 10 h. Ultimately, the above solution (1.5 mL) was added into silica nanoparticles (0.060 g) dispersed in anhydrous ethanol (20 mL) at 80 °C. The mixture was refluxed for 10 h under argon at this temperature. The core–shell luminescent nanoparticles were collected by centrifugation at a speed of 3500 rpm for 20 min, washed with acetone several times until the supernate did not present any lanthanide characteristic fluorescence under UV irradiation and dried at 60 °C in an oven for 20 h.

Synthesis of core–shell SiO_2@Ln(DPAE–Si)$_3$@NH_2 nanostructures (Ln = Eu^{3+} and Tb^{3+})

To 20 mL of ethanol were added 10 mL of aqueous solution containing SiO_2@Ln–DPAE (0.070 g) and 1.8 mL of ammonia. The solution was stirred for 30 min at room temperature. Then APTES (0.15 mL) dispersed in ethanol (20 mL) was added into the above solution and the mixture was further stirred for 5 h. The white precipitate was isolated by centrifugation, washed with water and ethanol four times, and dried at 60 °C for 10 h.

Acknowledgements

The authors are grateful to the CICS (Centre Imagerie Cellulaire Santé) of Clermont-Ferrand for TEM analysis.

Notes and references

1 (*a*) A. Bhirde, J. Xie, M. Swierczewska and X. Chen, *Nanoscale*, 2011, **3**, 142; (*b*) J. Rosenholm, C. Sahlgren and M. Lindén, *J. Mater. Chem.*, 2010, **20**, 2707; (*c*) J. Yan, M. C. Estévez, J. E. Smith, K. Wang, X. He, L. Wang and W. Tan, *Nano Today*, 2007, **2**, 44; (*d*) D. Knopp, D. Tang and R. Niessner, *Anal. Chim. Acta*, 2009, **647**, 14; (*e*) C. Fang and M. Zhang, *J. Mater. Chem.*, 2009, **19**, 6258; (*f*) D. K. Kim and J. Dobson, *J. Mater. Chem.*, 2009, **19**, 6294; (*g*) Y. Pia, A. Burns, J. Kim, U. Wiesner and T. Hyeon, *Adv. Funct. Mater.*, 2008, **18**, 3758.

2 (*a*) A. Burns, H. Ow and U. Wiesner, *Chem. Soc. Rev.*, 2006, **35**, 1028; (*b*) L. Wang, K. Wang, S. Santra, X. Zhao, L. R. Hilliard, J. E. Smith, Y. Wu and W. Tan, *Anal. Chem.*, 2006, **78**, 647; (*c*) Y.-S. Lin and C. L. Haynes, *Chem. Mater.*, 2009, **21**, 3979.

3 (*a*) A. Burns, P. Sengupta, T. Zedayko, B. Baird and U. Wiesner, *Small*, 2006, **2**, 723; (*b*) M. Tan, Z. Ye, G. Wang and J. Yuan, *Chem. Mater.*, 2004, **16**, 2494; (*c*) J. Choi, A. Burns, R. Williams, Z. Zhou, A. Flesken-Nikitin, W. Zipfel, U. Wiesner and A. Niktin, *J. Biomed. Opt.*, 2007, **12**, 064007; (*d*) S. Santra, P. Zhang, K. Wang, R. Tapec and W. Tan, *Anal. Chem.*, 2001, **73**, 4988; (*e*) G. G. Condorelli, C. Tudisco, A. Motta, A. Di Mauro, F. Lupo, A. Gulino and I. L. Fragalà, *Eur. J. Inorg. Chem.*, 2010, 4121; (*f*) A. Di Mauro, F. Lupo, A. Gulino and I. L. Fragalà, *J. Mater. Chem.*, 2009, **19**, 3507.

4 (*a*) J. C. G. Bünzli and C. Piguet, *Chem. Soc. Rev.*, 2005, **34**, 1048; (*b*) J. Yu, L. Sun, H. Peng and M. I. J. Stich, *J. Mater. Chem.*, 2010, **20**, 6975; (*c*) C. Andraud and O. Maury, *Eur. J. Inorg. Chem.*, 2009, 4357; (*d*) S. Pandya, J. Yu and D. Parker, *Dalton Trans.*, 2006, 2757.

5 E. G. Moore, A. P. S. Samuel and K. N. Raymond, *Acc. Chem. Res.*, 2009, **42**, 542.

6 (*a*) X. Guo, H. Guo, L. Fu, H. Zhang, L. D. Carlos, R. Deng and J. Yu, *J. Photochem. Photobiol., A*, 2008, **200**, 318; (*b*) K. Binnemans, *Chem. Rev.*, 2009, **109**, 4283.

7 (*a*) J. Hovinen and P. M. Guy, *Bioconjugate Chem.*, 2009, **20**, 404; (*b*) S. Poupart, C. Boudou, P. Peixoto, M. Massonneau, P.-Y. Renard and A. Romieu, *Org. Biomol. Chem.*, 2006, **4**, 4165; (*c*) A.-C. Franville, D. Zambon, R. Mahiou and Y. Troin, *Chem. Mater.*, 2000, **12**, 428; (*d*) A. Picot, A. D'Aleo, P. L. Baldeck, A. Grichine, A. Duperray, C. Andraud and O. Maury, *J. Am. Chem. Soc.*, 2008, **130**, 1532.

8 (*a*) Z. El A. Chamas, X. Guo, J.-L. Canet, A. Gautier, D. Boyer and R. Mahiou, *Dalton Trans.*, 2010, **39**, 7091; (*b*) O. Wallac and J. Hovinen, WO/2008/025886, 2008; (*c*) C. S. Bonnet, F. Buron, F. Caillé, C. M. Shade, B. Drahos, L. Pellegatti, J. Zhang, S. Villette, L. Helm, C. Pichon, F. Suzenet, S. Petoud and E. Toth, *Chem.–Eur. J.*, 2012, **18**, 1419.

9 (*a*) C. W. Tornøe and M. Meldal, in *Peptides: The Wave of the Future*, ed. M. Lebland R. A. Houghten, Kluwer Academic Publishers, Dordrecht, 2001, p. 263; (*b*) H. C. Kolb, M. G. Finn and K. B. Sharpless, *Angew. Chem., Int. Ed.*, 2001, **40**, 2004; (*c*) Z. P. Demko and K. B. Sharpless, *Org. Lett.*, 2001, **3**, 4091.

10 (*a*) J. Zhang, X. Wang, D. Wu and L. Liu, *Chem. Mater.*, 2009, **21**, 4012; (*b*) H. C. Kolb and K. B. Sharpless, *Drug Discovery Today*, 2003, **24**, 1128; (*c*) A. Maisonial, P. Serafin, M. Traika, E. Debitton, V. Théry, D. J. Aitken, P. Lemoine, B. Viossat and A. Gautier, *Eur. J. Inorg. Chem.*, 2008, 298; (*d*) A. Qin, L. Tang, J. W. Y. Lam, C. K. W. Jim, Y. Yu, H. Zhao, J. Sun and Z. Tang, *Adv. Funct. Mater.*, 2009, **19**, 1891; (*e*) D. I. Rozkiewicz, D. Janczewski, W. Verboom, B. Jan Ravoo and D. N. Reinhoudt, *Angew. Chem.*, 2006, **118**, 5418.

11 F. J. Arriagada and K. Osseo-Asare, *J. Colloid Interface Sci.*, 1999, **211**, 210.

